Nanoscale

Accepted Manuscript

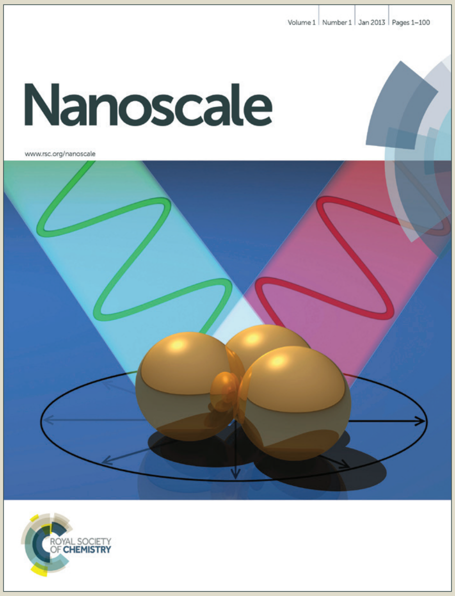

ROYAL SOCIETY OF CHEMISTRY

www.rsc.org/nanoscale

Cite this: DOI: 10.1039/c0xx00000x

www.rsc.org/xxxxxx

ARTICLE TYPE

Large-scale, solution-phase growth of semiconductor nanocrystals into ultralong one dimensional arrays and electrical properties

Yuchao Ma,[a] Mengmeng Xue,[a] Jiahua Shi[*b] and Yiwei Tan[*a]

Received (in XXX, XXX) Xth XXXXXXXXX 20XX, Accepted Xth XXXXXXXXX 20XX

DOI: 10.1039/b000000x

One-dimensional (1D) assemblies of semiconductor nanocrystals (NCs) represent an important kind of 1D nanomaterial systems due to their potential for exploring novel and enhanced electronic and photonic performances of devices. Herein, we present mass fabrication of a series of 1D arrays of CdSe and PbSe NCs on large length scale with ultralong, aligned Se nanowires (NWs) as both the reactant and structure-directed template. The 1D self-assembly patterns are the anchored growth of CdSe quantum dots (QDs) on the surface of Se NWs (i.e., 1D Se NWs/CdSe QDs core/shell heterostructure) and 1D aggregates of unsupported PbSe NCs formed by substantially increased collective particle–particle interactions. The size of CdSe QDs and shape of PbSe NCs in the 1D arrays can be effectively controlled by varying synthetic conditions. Room temperature electrical measurements on the 1D Se/CdSe heterostructure field effect transistors (FETs) exhibit the pronounced improvement in the on/off ratio, device carrier mobility, and transconductance compared to the Se NW FETs fabricated in parallel. Furthermore, upon visible light excitation, photocurrent from the Se/CdSe heterostructure FETs responses sharply (small time constant) and increases linearly with increasing the light intensity, indicating excellent photoconduction properties.

Introduction

Semiconductor NCs have been the subject of extensive experimental and fundamental theoretical investigations due to ever-expanding technological applications originating from their size- and shape-dependent electronic and optical properties.[1–4] The organization configuration of an ensemble of semiconductor NCs affords the programmable building blocks to diversify functionality of nanodevices. Thus far, the self-assembly of semiconductor NCs has been made substantial progress towards manipulating composition and structures/polymorphism of the self-assembled superstructures during past decades.[5–15] Unfortunately, the arrays of these semiconductor nanomaterials have been limited primarily to the format of either two- or three-dimensional superstructures on the limited length scale, while 1D patterned architectures of QDs or quantum rods is highly desirable such that one can carry forward the goal of the unidirectional enhancement of collective optical, optoelectronic, and energetic storage and conversion performance for developing novel electronic devices.[16,17] However, there is a great challenge in integrating an ensemble of discrete semiconductor NCs into 1D assemblies for the difficulties in creating unidirectional inter-particle interactions. In this aspect, only few examples were described previously in the literature, which were achieved by attaching NCs onto the regular 1D supports, such as carbon nanotubes or semiconductor NWs.[18–29]

The formation of 1D arrays of an ensemble of nanoparticles on a given surface generally involves postsynthesis organization of nanoparticles through templates or anisotropic interactions.[7,16,17] However, despite the significant progress in linear assemblies of various nanoparticles, such as metallic, semiconducting, and magnetic, those assembling processes were stepwise and cumbersome. Particularly, the large-scale, long-range 1D assembly of NCs is very hard to handle by controlling solvent evaporation, eternal field force, bonding cement molecules, and even in the presence of templates. This renders large-scale production and reproducibility of methods more elusive. Obviously, the development of bottom-up synthesis techniques for the straightforward 1D assembly of NCs is preferable since templating as well as engineering of nanoparticle surface should be dispensed easily. In this work, we report for the first time a one-pot, large-scalable synthesis of linearly integrated semiconductor NCs, including CdSe and PbSe, in aligned bundle arrangement at high outputs and on the millimetre length scale. In comparison to the limitations of those assemblies of QDs on misaligned carbon nanotubes or NWs, including low-throughput and short length scale,[18–29] we use the well-aligned, ultralong Se NWs bundles as the Se source and interconnects to facilitate combining the interface-anchored/embedded growth with unidirectional positioning and integration of individual semiconductor NCs. Thus, the 1D arrays of semiconductor NCs, which are exempt from self-entanglement, strikingly have a macroscopic length scale while remaining well aligned 1D layout.

Se NWs have been served as a reactive template to grow continuous and integral nanostructures, such as nanotubes, NWs, and Se–selenide core–shell heterostructures.[30–34] However, in this way, it is still technically challenging to synthesize tiny-sized, discrete NCs assembled into 1D-architectures. For growing semiconductor NCs, Se or Te NWs are preferable since they could provide high reactivity and be directly used as growing templates. The critical issue of our method to producing linear arrays of semiconductor NCs is the control of reaction extent of the disproportionation of Se NWs to Se^{2-} (i.e., CdSe and PbSe) and SeO_3^{2-} in order to prevent Se NWs from neither breaking nor entirely being consumed during the growth of semiconductor NCs. Meanwhile, to avoid monolithic growth of continuous and integral nanostructures, a coordinating solvent, oleic acid (OA), is used to appropriately passivate the surface of Se NWs so that the growth of semiconductor NCs occurs at some specific sites of the surface rather than over the entire surface, i.e., in a manner of pinhole effects. Furthermore, oleic acid serves as the capping ligand to control the shape and size of semiconductor NCs. Using this protocol, we have been able to synthesize 1D Se NWs/CdSe QDs core/shell (briefly, 1D Se/CdSe) heterostructure with QD size tunability and uniformity. To demonstrate the flexibility and generality of our method in the control of the assembled structure of semiconductor NCs, we also exemplify the linear self-assemblies of unsupported PbSe NCs (viz., without Se moiety) with a different shape by completely consuming Se NWs through combining reaction with dissolution in the presence of an appropriate solvent. The directional interparticle interactions are the underlying directive force for the linear self-assemblies, in lieu of the 1D supports including NWs or carbon nanotubes.

Unlike the assemblies of QDs on the 1D supports by van der Waals adsorption, where the attachment of colloidal QDs is mostly bridged via the linker molecules, 1D Se/CdSe heterostructure reported in this paper indicates that anchoring of semiconductor NCs on Se NWs enables new opportunities for studies on the structural, optical, and electrical properties of the 1D heterostructure of NCs binding with semiconductor NWs. In particular, compared to attachment of semiconductor NCs to carbon nanotubes or various NWs, there are important advantages of utilizing the 1D Se/CdSe heterostructure as an element for electric devices. First, the epitaxial growth of CdSe QDs on Se NWs provides robust binding between them, thereby ensuring the stability of optoelectrical performance. Second, controlled doping of Se NWs is feasible. As compared to the poor conductivity of core NWs, such as ZnO, SnO_2, and CdSe, as well as the diameter- and helicity-dependent conductivity of carbon nanotubes,[35,36] a desirable and specific conducting behaviour can thus be readily available. Third, Se NWs and CdSe QDs themselves have pronounced photoconductive properties. Therefore, herein, we focus on the electrical transport and optoelectrical properties of the 1D Se/CdSe heterostructure field effect transistors (FETs) aiming at introducing unique electronic and photonic function to circuit elements and devices.

Results and discussion

For preparing ultrahigh aspect ratio 1D arrays of semiconductor NCs, we first synthesized Se NWs on the millimetre length scale by the reduction of selenic acid using 2-methoxy-5-nitroaniline as the reductant under solvothermal conditions. This approach allows for large-scale production of high-purity Se NWs in high yield (81%). The crystalline structure of the Se NWs is characterized by powder X-ray diffraction (XRD) pattern (Fig. 1a), in which all the Bragg peaks can be perfectly indexed to pure *t*-Se (JCPDF no. 06-0362). Scanning electron microscopy (SEM) observations reveal that the as-prepared single Se NWs have lengths extending up to 1 mm and form ultralong, well-aligned bundles (Fig. 1b,c). Transmission electron microscopy (TEM) studies demonstrate that the Se NWs in the self-organized architectures have a very narrow diameter distribution and an average diameter of ~150 nm (Fig. 1d). Surveys of many Se NWs in the self-organized pattern using high resolution TEM (HRTEM) and selected area electron diffraction (SAED) suggest that Se NWs are constantly single crystal grown along the same crystallographic growth direction. The HRTEM image in Fig. 1e exhibits the Se NW with well-resolved (001) and (100) lattice planes. Fig. 1f shows the corresponding SAED pattern. HRTEM and the assignments of SAED consistently indicate that the preferential growth direction for Se NWs is [001].

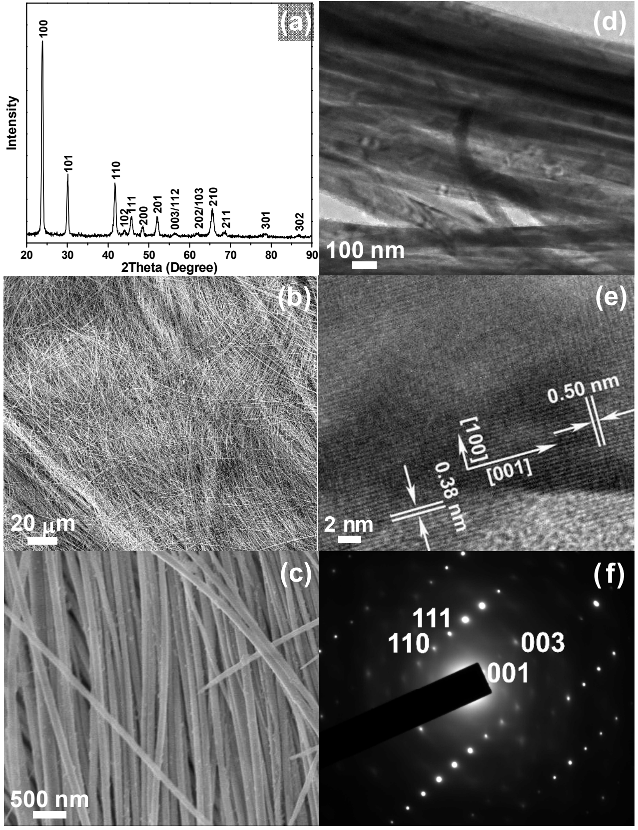

Fig. 1 (a) Powder XRD pattern, (b) low- and (c) high-magnification SEM, (d) TEM, and (e) HRTEM images of the aligned Se NW bundles prepared by using 2-methoxy-5-nitroaniline as the reductant in a cosolvent of pyridine and water at a volumetric ratio of 7/1 under solvothermal conditions. (f) The corresponding SAED pattern of the Se NW shown in panel e.

Se NWs are converted to CdSe or PbSe NCs by annealing them in OA or a mixed solvent of OA and squalane (v/v, 1/5) in the presence of $Cd(OH)_2$ or PbO, respectively. The extremely thick Se NWs are favourable for retaining their 1D nanostructures while

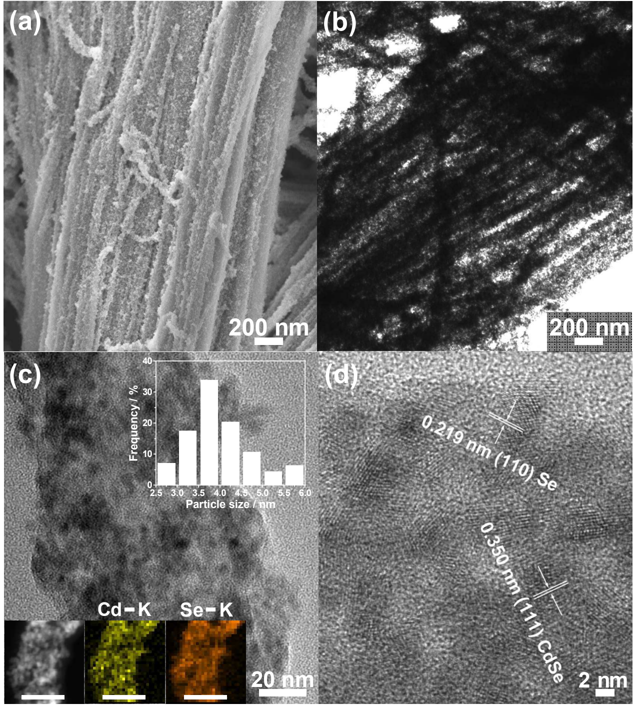

Fig. 2 (a) SEM and (b) low-magnification TEM images of a bundle of 1D CdSe/Se heterostructure. (c) High-magnification TEM and (d) HRTEM images of the CdSe NCs on a single Se NW. The top inset in panel c shows the corresponding size-distribution histogram of the CdSe NCs. The corresponding HAADF-STEM (left) and elemental mapping (right) images are shown in the bottom insets in panel c. Scale bars correspond to 50 nm. The growth of CdSe NCs on the surface of Se NWs was performed in 10 mL of OA at 165 ºC.

raising reaction temperature to enable the conversion of Se NWs to high crystalline semiconductor NCs, despite the low melting point of elemental Se (217 ºC). SEM image in Fig. 2a displays that the cylindrical strand-like fibres with a rough surface have been developed after Se NWs were treated with $Cd(OH)_2$ in 10 mL of OA at 165 ºC, indicating the formation of a large number of single CdSe NCs on the surface of each Se NW. Noted that many strands are bound together into closely packed bundle-like arrangements with lengths close to ~1 mm. Examination of the bundles by TEM analysis confirms that the well-aligned individual strands contain a large amount of nanoparticles with a narrow diameter distribution on their surface (Fig. 2b). High-magnification TEM image on the smaller length scale shows that each single strand is 90–125 nm in diameter and coated with numerous nearly monodisperse nanoparticles with an average size of 3.9 nm (Fig. 2c and the top inset therein). High-angle annular dark-field scanning TEM (HAADF-STEM) image clearly revealing the enhanced elemental contrast on the surface of each NW indicates the growth of numerous NCs (the bottom-left inset in Fig. 2c). Furthermore, elemental mapping analyses on single 1D Se/CdSe heterostructure confirm that the discrete Cd signals are scattered nonuniformly at the surfaces and Se is homogeneously distributed throughout the NWs (the bottom-right insets in Fig. 2c), implying the NW-core/QD-shell structure. The HRTEM imaging reveals single crystalline features and cubic zinc blende structure for the CdSe QDs in all the strands (Fig. 2d and Fig. S1a, ESI†), in which (111) lattice fringes are well resolved. Notably, no free-standing discrete, scattered QDs outside the 1D arrays are observed. The lattice fringes from (110) plane of Se NWs can also be identified in the HRTEM images, although they are not well resolved due to the different focal plane location. This clearly suggests the successful synthesis of well-defined 1D Se/CdSe heterostructure. The retention of crystalline Se NW substrate offers the outstanding unidirectional conductance for the linearly arrayed CdSe NCs.

The size of CdSe QDs on Se NWs can be easily tuned by varying reaction temperature or the volume of OA (V_{OA}). If the reaction is carried out in 10 mL of OA at 150 ºC, the fine CdSe NCs with an average diameter of 3.2 nm supported on the ultralong Se NWs are generated with the reaction progression (Fig. 3a–c). These CdSe NCs not only present sharp size distributions, but form a monolayer coating on the surface of Se NWs (Fig. S1b, ESI†). Also, the remains of Se NW species retain the crystalline structure. In contrast, a decrease in the V_{OA} leads to the production of the larger CdSe NCs with an average size of 8.3 nm on Se NWs (Fig. 3d–f and S1c, ESI†). As shown in Fig. 4, the XRD pattern of each sample confirms CdSe NCs in the cubic zinc-blende phase (a = 6.05 Å, JCPDS File, no. 65-2891). The mean grain size of CdSe NCs is calculated to be 3.0, 3.6, and 8.5 nm, respectively, in terms of Debye-Scherrer's formula, which is consistent with the particle size obtained on the basis of TEM analysis. At the same time, the reflection peaks from Se moiety can also be clearly identified.

Our strategy can be effectively extended to fabricate 1D self-assemblies of other semiconductor NCs on large scale. Low-magnification TEM overviews in Fig. 5a and S2a (ESI†) exclusively illustrate 1D arrays of PbSe NCs over a large length scale of more than hundreds of micrometres, where PbSe NCs are synthesized by the reaction of Se NWs with PbO in OA and squalane (v/v, 1/5). Fig. 5b shows an enlarged view of the marked area in Fig. 5a, in which the overwhelming majority of PbSe NCs are closely packed together and self-assembled into 1D bundles (also see Fig. S2b, ESI†). The stained domains around the bundles of PdSe NCs, showing dark contrast in TEM images, originate from the surfactant coating since no excess washing was applied to avoid modification or disruption of the 1D nanostructures. In addition, there are very few 1D chains of single PbSe NCs. The PbSe NCs have a cubic morphology and relatively uniform size distribution. The edge length of PbSe nanocubes is mostly in the range of 10–20 nm. The HRTEM images unambiguously reveal the cubic rock salt structure of PbSe, as shown with the fringe spacing of 2.17 Å, corresponding to lattice planes of (220) (Fig. 5c and S2c, ESI†). Additionally, no pristine Se NW substrate can be identified. In our case, instead of contiguous monolithic growth of PbSe NWs or nanorods through oriented attachment (i.e., rather than fusion of the 1D aggregates),[37–39] TEM and HRTEM images clearly reveal the grain boundary of PbSe nanocubes in the linked chains (Fig. 5b and 5c). HRTEM observations also provide the information on the nonalignment of the atomic lattices of the individual NCs. Furthermore, HAADF-STEM studies demonstrate that the PbSe NCs are in a consistent orientation with respect to one another neither in the bundles nor in the single chains. Representatively, HAADF-STEM image in the inset of Fig. 5d shows the (110) and (001) plane parallel to the substrate surface, as indicated by white and red arrows, respectively. XRD pattern of the linearly arrayed PbSe nanocubes confirms that all of the diffraction peaks can be assigned to the cubic rock-salt structure (Fig. 5d). No discernible peaks of Se NWs are observed, apparently because the squalane promote the dissolution and conversion of Se NWs.[38]

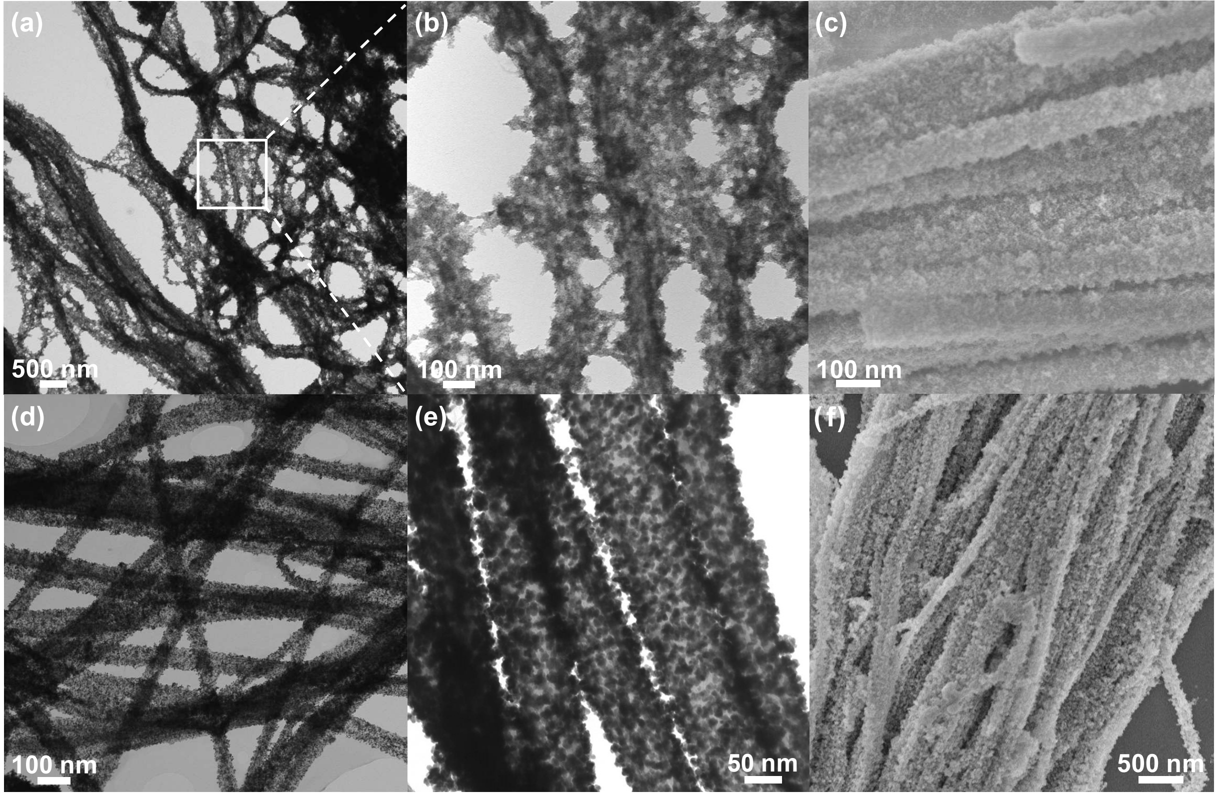

Fig.3 (a and d) Low-magnification TEM, (b and e) high-magnification TEM, and (c and f) SEM images of the 1D arrays of CdSe NCs with a different average size grown on the surface of Se NWs. Experimental conditions for control of the size of CdSe NCs: (a–c) 10.0 mL of OA at 150 ºC; (d–f) 8.0 mL of OA at 150 ºC.

Furthermore, the shape of PbSe NCs for constructing 1D self-assembly can be tunable by changing the synthetic conditions. Fig. 5e displays the SEM image of the large-scale 1D strands composed of the PbSe nanorods obtained by introducing an additional surfactant tris(diethylamino)phosphine into the reaction system (also see Fig. S3a, ESI†). In comparison to the 1D arrays of PbSe nanocubes, the 1D structure and dimension formed by the self-assembly of nanorods change significantly. These self-assembled 1D strands with high affinity between one another are uniaxially aligned and bind together laterally into a huge chunk-like superstructure, thus indicating very strong interactions among them. The enlarged SEM images show that the long axes of the constituent nanorods inside each strand are aligned nearly along the strand (Fig. S3b, ESI†). As shown in the TEM image (Fig. 5f and the inset therein), the nanorods have a large size, with an average length of 170 nm and an aspect ratio of about 5. It can be seen that the PbSe nanorods still bind tightly together and pack side-by-side in the 1D strands while the self-assembled structure has been ultrasonicated for full dispersion prior to the TEM examination.

In our case, the growth of semiconductor NCs occurs at the solid/liquid interface. In contrast to the dissolved Se molecules that are extensively used as the Se source in the homogeneous solutions, the use of Se NWs is unique in the control of size and shape of semiconductor NCs. Compared to those previous high-temperature growth processes via hot injection technique,[40–45] the low reactive temperatures and small contact area between the reactive precursors (i.e., Se atoms and Cd^{2+}/OA ligands) at the surface of Se NWs significantly reduce the reaction rate. In particular, the growth of semiconductor NCs on Se NWs is based on the pinhole effect. Thus, our experimental conditions explicitly determine the reaction-controlled growth of semiconductor NCs. Unlike the conventional diffusion-limited growth,[40–42] this is the first experimental operation of a reaction-controlled process in the focusing of size and shape of distribution of semiconductor NCs.

In spite of complete consumption of Se NWs, nearly no scattered PbSe NCs are visible. It should be noted that the most prominent feature of the self-assembled 1D PbSe NCs is that the self-assembled 1D structures are free-standing and independent of the underlying substrate. Apparently, the linear self-organization of PbSe NCs should result from the long-range axial attraction due to their soft surface invoked by the OA ligand-passivated facets of PbSe NCs. The interaction energies (E) among PbSe NCs in the 1D arrays might involve the dipole–

dipole (E_d) and van der Waals (E_w) attraction, and quadrupolar repulsion (E_q) gained by bringing NCs in close contact with one another. The total energy may be expressed as:

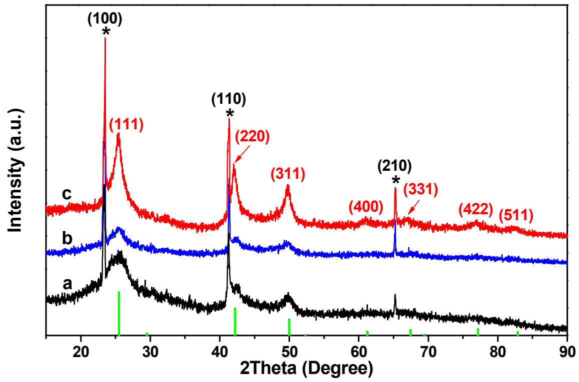

Fig. 4 Powder X-ray diffractograms of the heterostructure of 1D CdSe QDs on Se NWs synthesized in (a) 10 mL of oleic acid at 150 °C, (b) 10 mL of oleic acid at 165 °C, and (c) 8 mL of oleic acid at 150 °C. The reflection peaks labelled with asterisks are assigned to Se NWs.

$$E = E_\mathrm{d} + E_\mathrm{w} - E_\mathrm{q} \qquad (1)$$

wherein the long-range attraction accounting for the 1D self-assembly results from the dipole–dipole interactions. If the particulate centre-to-centre distance of R (i.e., for the non-neighbouring particles) is much larger than the dimension of the particle radius a, the size-scaling of the dipole–dipole and quadrupolar interactions between particles in reaction medium is described as:[46]

$$E_\mathrm{d} - E_\mathrm{q} = c_1\left(\frac{a^4}{R^3}\right) - c_2\left(\frac{a^6}{R^5}\right) \qquad (2)$$

where c_1 and c_2 are constants to be determined. This is because the dispersion of the aligned PbSe NC bundles that are growing is approximately considered as a nematic host fluid due to the dissolution of Se NWs in the presence of squalane. Therefore, for larger cubic and rodlike particles, the quadrupole term becomes important and the quadrupolar repulsion energy takes effects in a sufficiently short range and decays rapidly as R^{-5}. Unlike single particle chains, the larger repulsion force among multiple PbSe NCs over a short range leads to the particle clusters assuming angles at intervals relative to longitudinal axis of each 1D bundle. Thus, kinked or bended 1D bundles are formed that are much more prevalent than the straight chains.

At the same time, we propose that the packing pattern of the surfactant molecules on the surface of PbSe NCs induces anisotropic spatial charge distribution, which is responsible for the enhanced electric dipole moment for the ultralong 1D self-assemblies of PbSe NCs. Note that PbSe NCs are allowed to nucleate and grow in the regime of limited surface dimension of Se NW templates, which renders the close contact among the growing PbSe NCs. This thereby facilitates their electronic interaction and in turn promotes globally anisotropic attraction. The surface coverage of OA is often rather low on the two adjacent NC surfaces in the case of a distance between the neighbouring NCs smaller than the length of the OA, due to the depletion effect,[47] so that the spatial bias of capping ligand intensifies the surface charge anisotropy. The intrinsic polar facets of PbSe NCs[48] tend to bind together through a high density of unpassivated surface states in the region between the neighbouring NCs. Similarly, loss of ligand OA caused by solvent treatments leads to both the greater dipole–dipole coupling and wave function overlap effects between PbSe NCs, as stated in the recent literature.[49,50] Particularly, the lateral coupling of multiple NCs into clusters greatly enhances the dipole–dipole interactions as a result of summing multiple dipole moments. In addition, the 1D self-assemblies are driven by the entropy

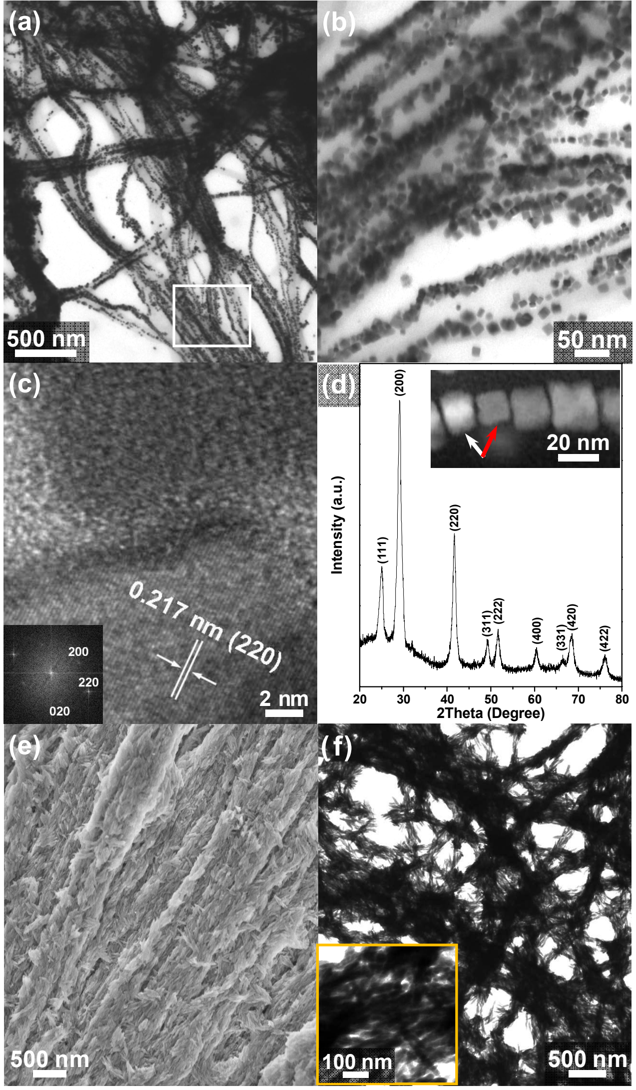

Fig. 5 (a) Low-magnification TEM image of bundles of the 1D arrays of PbSe NCs. (b) A zoom-in view of the region marked in the panel a to permit closer examination of the PbSe NCs in the linear arrays. (c) HRTEM image and (d) XRD pattern of the PbSe nanocubes arrayed linearly. (e) SEM and (f) TEM images of the 1D arrays of PbSe nanorods. The insets in panels c, d, and f show the SAED pattern and STEM image of PbSe nanocubes, and the corresponding higher-magnification TEM view, respectively.

increase associated with the formation of burls of several PbSe NCs attached onto the sides of the 1D aggregates.

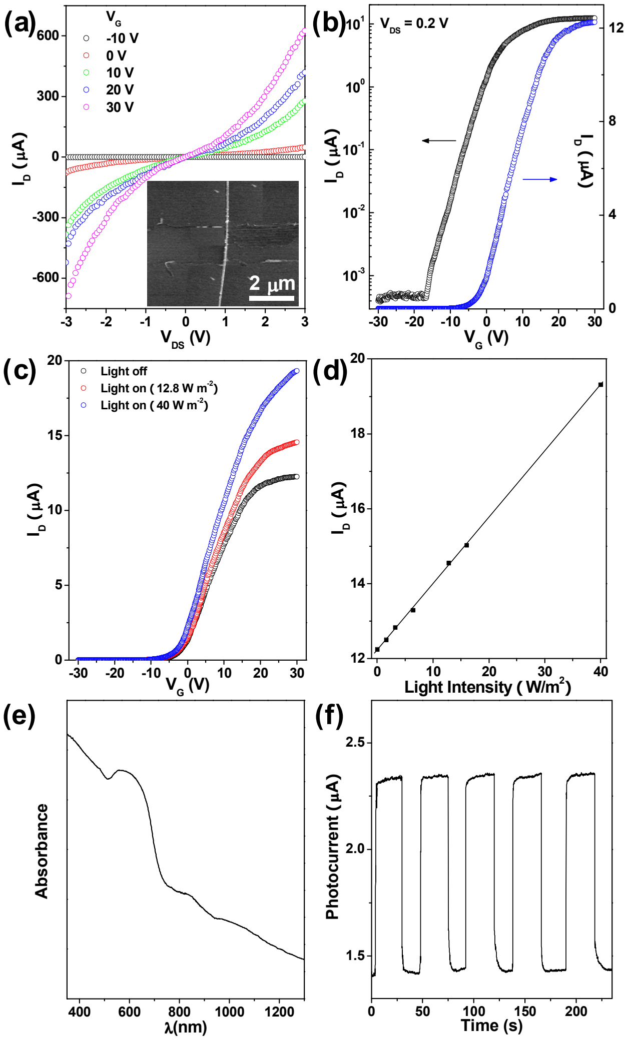

Fig.6 (a) Output characteristics (drain current I_D versus drain-source voltage V_{DS}) of the Se/CdSe FET device in the dark as a function of gate voltage V_G. (b) Plots of I_D versus V_G obtained at different V_G and constant V_{DS} of 0.2 V on logarithmic (black) and linear (blue) scales. (c) Transfer characteristics of the Se/CdSe FET device with light excitation (bias V_{DS} = 0.2 V). (d) Linear characteristics between photocurrent and the intensity (I) of illumination (I changing from 1.6 to 40 W m^{-2}) at bias 0.2 V and V_G = 30 V. (e) Optical absorption spectrum of the 1D Se/CdSe heterostructure. (f) Light response of the device as a function of time (bias 0.2 V). The inset in panel a shows the SEM image of the fabricated Se/CdSe FET device.

To fabricate the individual 1D Se/CdSe heterostructure field-effect transistors (FETs), an e-beam lithographic process was used to construct Au/Ti (50 nm/10 nm) source and drain electrodes on a SiO_2 (500 nm)/Si substrate. The 1D Se/CdSe heterostructure used for fabricating the FET devices are the sample shown in Fig. 2. The SEM image in the inset of Fig. 6a illustrates a typical nanodevice for the investigation on photoelectric properties of a single 1D Se/CdSe heterostructure. The plots of drain current I_D versus drain/source voltage V_{DS} are measured under a series of gate voltages V_G in steps of 10 V in the dark at room temperature, exhibiting linear regions at low V_{DS} (Fig. 6a). As determined by the slope of I_D–V_{DS} curves, the conductance of the field-effect device with the Se/CdSe heterostructure increases with increasing gate voltage from −10 to 30 V in steps of 10 V (Fig. 6a), showing an n-type FET.[51] Based on the slope of approximately linear regime of the I_D–V_{DS} curve obtained at V_G = 0 V, the conductivity of the Se/CdSe heterostructure with a diameter of 105 nm and spanning ca. 2 μm gap between drain and source electrodes is estimated to be ~26 Ω^{-1} cm^{-1}. This value is significantly larger than those of crystalline Se that is a p-type semiconductor and has conductivities in the range of 10^{-5}–10^{-6} Ω^{-1} cm^{-1} at room temperature.[52] For the 1D Se/CdSe heterostructure, its switching to n-type and increase in conductivity might be attributed to the doping effect from the formation of CdSe NCs. The transfer curve of the device shows a good current modulation characteristic, evidenced by an order of on/off ratio as high as 10^4 (off-current < 0.7 nA) (Fig. 6b). For comparison, the output (I_D *vs.* V_G) characteristics of the single Se NW FETs fabricated in parallel using Se NWs with nearly the same diameter and channel length were also measured at various gate voltages (Fig. S4a, ESI†). Similar to a previous investigation,[53] the I_{DS} *vs.* V_G curves for the Se NW device manifest a p-type semiconducting behaviour. Concomitantly, we estimate the conductivity of the Se NW as 0.05 Ω^{-1} cm^{-1}, which is 2 orders of magnitude lower than that of the Se/CdSe device (assuming zero contact resistance for both cases). The on-off ratio of the Se NW FETs is only on the order of 10^3 (Fig. S4b, ESI†), indicating a better current modulation for the Se/CdSe heterostructure after growing CdSe NCs on Se NWs. Note that the conductivity of our Se NWs is several orders of magnitude higher than that of the single crystal Se.[52] Considering that the conductivity of Se is drastically sensitive to the inclusion of impurities, this result is acceptable. In addition, it should be pointed out that the Se/CdSe FETs do not switch to an on-state at the negative gate voltage despite the Se moiety, that is, a non-analogue of a p-type FET device. This implies that sufficient electrons have been injected into the conduction band of Se NWs after the growth of CdSe NCs on their surface.

The linear regime field-effect mobility for electrons in the Se/CdSe heterostructure devices can be calculated from the slope in the transfer characteristics by the formula of transconductance $g_m = dI_{DS}/dV_G = \mu(C_g/L_g^2)V_{DS}$,[54,55] where a transconductance (g_m) of 0.63 μS, μ is the mobility, C_g is the gate capacitance, L_g is the length of the device (2 μm), and V_{DS} = 0.2 V. For a 105-nm diameter Se/CdSe heterostructure, C_g value can be estimated using the formula $C_g = 2\pi L\square\square_0/\ln(2h/r)$, where L and r are the length (2 μm) and radius (52.5 nm) of Se/CdSe heterostructure, respectively, and □ and h are the dielectric constant (~4.1) and gate dielectric thickness (500 nm) of SiO_2 layer, respectively. We evaluate the electron mobility of μ_e = 815 cm^2 V^{-1} s^{-1} for the 1D Se/CdSe heterostructure devices and a 1D electron density of 4.8 × 10^7 cm^{-1} (n = $C_gV_{G,Th}/eL$, $V_{G,Th}$ = −10 V (threshold voltage)). Such a large electron concentration suggests that the 1D Se/CdSe heterostructure is doped with donors, probably on account of the reaction processing. For comparison, the hole mobility and density are estimated to be 9 cm^2 V^{-1} s^{-1} and 4.9 × 10^7 cm^{-1}, respectively, for the Se NW devices. Therefore, our synthesis of CdSe NCs grown on Se NWs allows significant improvement of the device carrier mobility. The underlying mechanism for the improved FET performance of the Se/CdSe heterostructure versus Se NWs can be justified by the numerous heterojunctions with the dimensions of a few nanometres between the CdSe NCs and the Se NWs. The electrically charged Se-terminated {111} facets at the heterointerfaces between CdSe NCs and the Se NW core are expected to increase electron mobility due to the coupling of contact charging and electrostatic induction. This corresponds to the formation of a delocalized, extended state of a quantum confined electron near each dot heterostructure. Particularly, the electron mobility would be effectively regulated by changing the coverage of CdSe QDs on the Se NWs, which provides a different density of electron charge caused by the negatively charged, Se-terminated polar crystal facets.

The corresponding optical response profiles are shown in Fig. 6c. Remarkably, the photocurrent increases by 7.1 μA at V_G = 30 V upon light illumination in comparison with the value obtained in the dark. Ostensibly, the photocurrent can be assigned to the photoelectrons arising from both CdSe and Se moieties. However, the I_D–V_G characteristic curve of the single Se NW device shows photocurrent elevation by a small margin (0.67 μA at V_G = 30 V) (see Fig. S5, ESI†). In addition, the photo-generated electrons from CdSe QDs grown on Se NWs are not expected to increase so much considering the cases of CdSe QDs coating on carbon nanotubes.[56,57] Thus, we assume that photoexcitation would be increased with the generation of impurity energy level, due to both the synthetic reaction and the formation of the hybrid junction between the outer semiconducting CdSe NCs and the Se inner core. Accordingly, this could result in an increase in the allowed paths for photo-excitation. Correspondingly, the UV–vis absorption spectrum of the 1D Se/CdSe heterostructure shows broad absorption below 800 nm (in Fig. 6e), agreeing well with the much lower energy band gap of Se (~1.0–1.2 eV)[58] and impurities relative to CdSe.

Fig. 6d reveals that the photocurrent of the 1D Se/CdSe heterostructure devices increases linearly with an increase in light intensities from dark, 1.6, 3.2, 6.4, 12.8, and 16, to 40 W m^{-2} at bias 0.2 V and V_G = 30 V, reflecting the good sensitivity of photoelectron concentration of the devices to light. This also indicates enhanced photoresponse can be well controlled by a gate electrode. The device exhibits a photoconductivity as high as 23 Ω^{-1} cm^{-1} under the illumination intensity of 40 W m^{-2} (Fig. S6, ESI†), which is much higher than that (0.8 Ω^{-1} cm^{-1}) of Se NWs (Fig. S6, ESI†) and the reported value for 1D Se nanotubes.[59] Particularly, the photoconductivity of our 1D CdSe/Se heterostructure is superior to the pure CdSe NWs or nanotubes as a result of the poor electronic conductivity of CdSe itself.[60,61] Light excitation can induce an avalanche-like rise in photocurrent, as shown by photocurrent of the device *vs*. time monitored under 0 gate voltage (Fig. 6f). The photoresponse time (time constant) is less than 0.2 s supposing an exponential time dependence. The on and off current level remained nearly unchanged with time as well. The 1D CdSe/Se heterostructure facilitates electron transfer across the interface from CdSe to Se NW core and results in an equilibrium between the Fermi level of the CdSe and the Se NWs. As a consequence, an electrically charged layer and a built-in electric field are formed at the interface.

Conclusions

We have demonstrated effective routes to large-scale production of well-defined, ultralong 1D arrays of semiconducting NCs. The length of linearly assembled NCs can extend to *ca*. 1 mm. The size and shape of NCs in the 1D arrays can be effectively controlled. In particular, the particle–particle interactions are unique in the 1D self-assembly of PbSe NCs due to the growth in the surface-limited regime of Se NW templates and therefore affect the morphology of 1D array. Typically, 1D Se/CdSe heterostructure field-effect transistors are fabricated, which yields high-mobility n-type FETs. FET measurements exhibit excellent photoconductive properties. At the same time, the FETs are fairly stable, which exhibit almost the same responses to the FET measurements after six-month storage in glovebox filled with nitrogen. Our results indicate that the 1D Se/CdSe heterostructure FETs can provide the building blocks of complex complementary circuits for a range of applications in macroelectronics, sensors, and photoelectric conversion devices.

Experimental Section

Materials

All reagents were commercially available and used as received. Selenic acid (H_2SeO_4, 40% aq. soln.), 2-methoxy-5-nitroaniline (98%), squalane (98%), tris(diethylamino)phosphine (97%), pyridine (99%), 1-methyl-2-pyrrolidinone (99%), and 1-octadecene (90%) were purchased from Alfa Aesar. Cadmium hydroxide, lead(II) oxide, and oleic acid (OA, 90%) were purchased from Sigma-Aldrich. Anhydrous ethanol and hexane were purchased from other commercial sources.

Synthesis

Se NW templates. Typically, 0.8 mmol of 2-methoxy-5-nitroaniline was dissolved in 35.0 mL of pyridine, and then was mixed with 5.0 mL of an aqueous solution of H_2SeO_4 (0.08 M) in a 40 mL autoclave. The autoclave was sealed and maintained at 180 ºC for 10 h and subsequently cooled to ambient temperature naturally. The Se NWs are in the form of brown sediments at the bottom of autoclave. Concomitantly, the polymers produced after oxidation polymerization is well dissolved in the cosolvent of pyridine and water. Thus, the brown sediments can be facilely isolated by pouring off the supernatant polymer solution. The isolated Se NW sediments were alternately washed with 1-methyl-2-pyrrolidinone (10 mL) and ethanol (10 mL) for many times at 50 ºC to remove the adsorbed polymers on the surface of Se NWs. Ultimately, the Se NWs were washed with absolute ethanol (10 mL) for several times to get rid of any traces of 1-methyl-2-pyrrolidinone and then dispersed in 5 mL of absolute ethanol for various measurements and the subsequent syntheses of semiconductor NCs.

To prepare one dimensionally arrayed CdSe and PbSe NCs, all syntheses were carried out through a standard airless procedure, that is, under dry nitrogen atmosphere using standard Schlenk-line techniques with vigorous magnetic stirring.

1D self-assemblies of CdSe NCs on Se NWs. Typically, 33.4 mg (0.228 mmol) of Cd(OH)$_2$ was dissolved in 10.0 mL of OA at 100 ºC under vigorous stirring for 40 min. Subsequently, 9.0 mg (0.114 mmol) of Se NWs that were dispersed in 0.5 mL of ethanol was fed into this Cd(OH)$_2$ solution. After fully mixing the reactants for 20 min at the same temperature to allow the complete evaporation of ethanol, the reaction mixture was heated to 165 ºC and maintained at that temperature for 15 h. Once the reaction finished, the resultant mixture was cooled to ambient temperature naturally under nitrogen atmosphere. To adjust the CdSe NC size in the 1D arrays, either the volume of OA or reaction temperature was changed to 8.0 mL or 150 ºC, respectively, while keeping the other experimental parameters the same.

1D self-assemblies of free-standing PbSe NCs. Typically, 55.8 mg (0.25 mmol) of PbO was placed into a three-necked flask (100 mL) containing 1.0 mL of OA and 5.0 mL of squalane, which was connected to Schlenk line and evacuated air and refilled with nitrogen. The mixture was heat to 120 ºC for ca. 30 min under vigorous stirring until PbO was dissolved to form a clear solution. Subsequently, to the above mixture, 0.20 mL of diphenyl ether (or tris(diethylamino)phosphine) and 59.3 mg (0.75 mmol) of Se NWs dispersed in 0.5 mL of ethanol were injected. After drying under nitrogen at 120 ºC for 20 min, the reaction mixture, to which diphenyl ether or tris(diethylamino)-phosphine was added, was heated to 160 ºC and kept at that temperature for 10 h, or to 150 ºC and kept at that temperature for 30 min and then to 170 ºC and kept at that temperature for 10 min, respectively. Once the reaction finished, the above reaction mixtures were cooled naturally to room temperature.

The above various precipitated products were sequentially washed with ethanol and isolated by centrifugation (at 5000 rpm for 5 min) for many times, and then dispersed in hexane.

Measurements

Powder X-ray diffraction (XRD) patterns were recorded on a Rigaku Smartlab diffractometer with Cu Kα radiation (λ = 1.5406 Å) operated at 40 kV and 40 mA at a scanning rate of 6.0º min^{-1}. A Hitachi S-4800 field-emission scanning electron microscope (FESEM) operated at 5 kV was used for high resolution SEM imaging. Specimens for SEM studies were prepared by directly transferring the dispersion of purified products in hexane onto silicon slices. Transmission electron microscopy (TEM) images were taken on a JEOL-JEM-1010 transmission electron microscope operated at 80 kV. High-resolution TEM (HRTEM), HAADF-STEM, elemental mapping images, and selected area electron diffraction (SAED) patterns were taken on a FEI Tecnai G2 F20 S-Twin transmission electron microscope operated at 200 kV. Specimens for TEM and HRTEM observations were prepared by drop-casting the dispersion that has been shaken for a few minutes onto carbon-coated copper grids. Optical absorption spectrum was acquired with a Shimadzu UV-3600 spectrophotometer equipped with an integrating sphere. Field-effect measurements were performed with a four-probe station connected to Keithley 4200-SCS semiconductor analyzer in a shielded box at room temperature inside a N$_2$-filled glovebox. For the light response measurements of the FET device, the light source used is a light-emitting diode (LED) with an excitation wavelength (λ_{ex}) of 400 nm.

Acknowledgements

This work was financially supported by the National Natural Science Foundation of China (No. 21071079, 21371097, 21073054) and the Research Fund of State Key Laboratory of Materials-Oriented Chemical Engineering (2009, 2012 (ZK201209)).

Notes and references

[a] *State Key Laboratory of Materials-Oriented Chemical Engineering, School of Chemistry and Chemical Engineering, Nanjing Tech University, Nanjing, 21009, China. Tel: +86-25-83172267; E-mail: ytan@njtech.edu.cn*

[b] *Key Laboratory of Natural Medicine and Immuno-Engineering of Henan Province, Henan University, Kaifeng 475004, China, Email: sjiahua@henu.edu.cn*

† Electronic Supplementary Information (ESI) available: more characterization results. See DOI: 10.1039/b000000x/

1 C. B. Murray, C. R. Kagan and M. G. Bawendi, *Annu. Rev. Mater. Sci*., 2000, **30**, 545–610.
2 M. A. El-Sayed, *Acc. Chem. Res*., 2004, **37**, 326–333.
3 D. V. Talapin, J.-S. Lee, M. V. Kovalenko and E. V. Shevchenko, *Chem. Rev*., 2010, **110**, 389–458.
4 P. Zrazhevskiy, M. Senawb and X. Gao, *Chem. Soc. Rev*., 2010, **39**, 4326–4354.
5 C. B. Murray, C. R. Kagan and M. G. Bawendi, *Science*, 1995, **270**, 1335–1338.
6 E. V. Shevchenko, D. V. Talapin, N. A. Kotov, S. O'Brien and C. B. Murray, *Nature*, 2006, **439**, 55–59.
7 T. Wang, D. LaMontagne, J. Lynch, J. Zhuang and Y. C. Cao, *Chem. Soc. Rev*., 2013, **42**, 2804–2823.
8 T. Wang, J. Zhuang, J. Lynch, O. Chen, Z. Wang, X. Wang, D. LaMontagne, H. Wu, Z. Wang and Y. C. Cao, *Science*, 2012, **338**, 358–363.
9 F. X. Redl, K.-S. Cho, C. B. Murray and S. O'Brien, *Nature*, 2003, **423**, 968–971.
10 S. Ahmeda and K. M. Ryan, *Chem. Commun*., 2009, 6421–6423.
11 M. Zanella, G. Bertoni, I. R. Franchini, R. Brescia, D. Baranov and L. Manna, *Chem. Commun*., 2011, **47**, 203–205.
12 S. M. Rupich, E. V. Shevchenko, M. I. Bodnarchuk, B. Lee and D. V. Talapin, *J. Am. Chem. Soc*., 2010, **132**, 289–296.
13 W. H. Evers, B. De Nijs, L. Filion, S. Castillo, M. Dijkstra and D. Vanmaekelbergh, *Nano Lett.*, 2010, **10**, 4235–4241.
14 T. Huang, Q. Zhao, J. Xiao and L. Qi, *ACS Nano*, 2010, **4**, 4707–4716.
15 Y. Wang, Q. Dai, B. Zou, W. W. Yu, B. Liu and G. Zou, *Langmuir*, 2010, **26**, 19129–19135.
16 Z. Tang and N. A. Kotov, *Adv. Mater*., 2005, **17**, 951–962.
17 H. Kitching, M. J. Shiers, A. J. Kenyon and Ivan P. Parkin, *J. Mater. Chem. A*, 2013, **1**, 6985–6999.
18 Q. Li, B. Sun, I. A. Kinloch, D. Zhi, H. Sirringhaus and A. H. Windle, *Chem. Mater*., 2006, **18**, 164–168.
19 C. Engtrakul, Y.-H. Kim, J. M. Nedeljković, S. P. Ahrenkiel, K. E. H. Gilbert, J. L. Alleman, S. B. Zhang, O. I. Mićić, A. J. Nozik and M. J. Heben, *J. Phys. Chem. B*, 2006, **110**, 25153–25157.
20 Y. J. Na, H. S. Kim and J. Park, *J. Phys. Chem. C*, 2008, **112**, 11218–11226.
21 B. H. Juárez, M. Meyns, A. Chanaewa, Y. Cai, C. Klinke and H. Weller, *J. Am. Chem. Soc*., 2008, **130**, 15282–15284.
22 C. Lu, A. Akey, W. Wang and I. P. Herman, *J. Am. Chem. Soc*., 2009, **131**, 3446–3447.
23 D. G. Ramlan, S. J. May, J.-G. Zheng, J. E. Allen, B. W. Wessels and L. J. Lauhon, *Nano Lett*., 2006, **6**, 50–54.

24 M. L. Lu, C. H. Lin and Y. F. Chen, *Appl. Phys. Lett*., 2011, **99**, 081109.

25 K. S. Leschkies, R. Divakar, J. Basu, E. Enache-Pommer, J. E. Boercker, C. B. Carter, U. R. Kortshagen, D. J. Norris and E. S. Aydil, *Nano Lett*., 2007, **7**, 1793–1798.

26 G. Wang, X. Yang, F. Qian, J. Z. Zhang and Y. Li, *Nano Lett*., 2010, **10**, 1088–1092.

27 D. Hou, A. Dev, K. Frank, A. Rosenauer and T. Voss, *J. Phys. Chem*. C, 2012, **116**, 19604–19610.

28 Q. Dai, J. Chen, L. Lu, J. Tang and W. Wang, *Nano Lett*., 2012, **12**, 4187–4193.

29 Y. Yu, P. V. Kamat and M. Kuno, *Adv. Funct. Mater*., 2010, **20**, 1464–1472.

30 B. Gates, Y. Wu, Y. Yin, P. Yang and Y. Xia, *J. Am. Chem. Soc*., 2001, **123**, 11500–11501.

31 B. Mayers, X. Jiang, D. Sunderland, B. Cattle and Y. Xia, *J. Am. Chem. Soc*., 2003, **125**, 13364–13365.

32 X. Jiang, B. Mayers, T. Herricks and Y. Xia, *Adv. Mater*., 2003, **15**, 1740–1743.

33 H.-W. Liang, S. Liu, J.-Y. Gong, S.-B. Wang, L. Wang and S.-H. Yu, *Adv. Mater*., 2009, **21**, 1850–1854.

34 H.-W. Liang, S. Liu and S.-H. Yu, *Adv. Mater*., 2010, **22**, 3925–3937.

35 J. W. G. Wildoer, L. C. Venema, A. G. Rinzler, R. E. Smalley and C. Dekker, *Nature*, 1998, **391**, 59–62.

36 T. W. Odom, J.-L. Huang, P. Kim and C. M. Lieber, *Nature*, 1998, **391**, 62–64.

37 K. S. Cho, D. V. Talapin, W. Gaschler and C. B. Murray, *J. Am. Chem. Soc*., 2005, **127**, 7140–7147.

38 W.-k. Koh, A. C. Bartnik, F. W. Wise and C. B. Murray, *J. Am. Chem. Soc*., 2010, **132**, 3909–3913.

39 W. H. Evers, B. Goris, S. Bals, M. Casavola, J. de Graaf, R. van Roij, M. Dijkstra and D. Vanmaekelbergh, *Nano Lett*., 2013, **13**, 2317–2323.

40 X. Peng, J. Wickham and A. P. Alivisatos, *J. Am. Chem. Soc*., 1998, **120**, 5343–5344.

41 Z. A. Peng and X. Peng, *J. Am. Chem. Soc*., 2001, **123**, 1389–1395.

42 Z. A. Peng and X. Peng, *J. Am. Chem. Soc*., 2002, **124**, 3343–3353.

43 B. K. H. Yen, N. E. Stott, K. F. Jensen and M. G. Bawendi, *Adv. Mater*. 2003, **15**, 1858–1862.

44 C. R. Bullen and P. Mulvaney, *Nano Lett*. 2004, **4**, 2303–2307.

45 L. Liu, Z. Zhuang, T. Xie, Y.-G. Wang, J. Li, Q. Peng and Y. Li, *J. Am. Chem. Soc*., 2009, **131**, 16423–16429.

46 T. C. Lubensky, D. Pettey, N. Currier and H. Stark, *Phys. Rev. E*, 1998, **57**, 610–625.

47 S. Asakura and F. Oosawa, *J. Chem. Phys*. 1954, **22**, 1255–1256.

48 J.-X. Ma, Y. Jia, Y.-L. Song, E.-J. Liang, L.-K. Wu, F. Wang, X.-C. Wang and X. Hu, *Surf. Sci*., 2004, **551**, 91–98.

49 J. M. Luther, M. Law, Q. Song, C. L. Perkins, M. C. Beard and A. J. Nozik, *ACS Nano*, 2008, **2**, 271–280.

50 M. Law, J. M. Luther, Q. Song, B. K. Hughes, C. L. Perkins and A. J. Nozik, *J. Am. Chem. Soc*., 2008, **130**, 5974–5985.

51 Y. Cui, X. Duan, J. Hu and C. M. Lieber, *J. Phys. Chem. B*, 2000, **104**, 5213–5216.

52 K. E. Murphy, B. B. Wunderlich and B. Wunderlich, *J. Phys. Chem*., 1982, **86**, 2827–2835.

53 D. Qin, H. Tao, Y. Zhao, L. Lan, K. Chan and Y. Cao, *Nanotechnology*, 2008, **19**, 355201.

54 R. Martel, T. Schmidt, H. R. Shea, T. Hertel and Ph. Avouris, *Appl. Phys. Lett*., 1998, **73**, 2447–2449.

55 X. Jiang, Q. Xiong, S Nam, F. Qian, Y. Li and C. M. Lieber, *Nano Lett*., 2007, **7**, 3214–3218.

56 L. Hu, Y.-L. Zhao, K. Ryu, C. Zhou, J. F. Stoddart and G. Grüner, *Adv. Mater*., 2008, **20**, 939–946.

57 K. Yu, G. Lu, K. Chen, S. Mao, H. Kim and J. Chen, *Nanoscale*, 2012, **4**, 742–746.

58 M. U. Kahaly, P. Ghosh, S. Narasimhan and U. V. Waghmare. *J. Chem. Phys*., 2008, **128**, 044718-1–10.

59 P. Liu, Y. Ma, W. Cai, Z. Wang, J. Wang, L. Qi and D. Chen, *Nanotechnology*, 2007, **18**, 205704.

60 S.-C. Kung, W. Xing, W. E. van der Veer, F. Yang, K. C. Donavan, M. Cheng, J. C. Hemminger and R. M. Penner, *ACS Nano*, 2011, **5**, 7627–7639.

61 D. Yu, C. Wang and P. Guyot-Sionnest, *Science*, 2003, **300**, 1277–1280.

Table of Contents

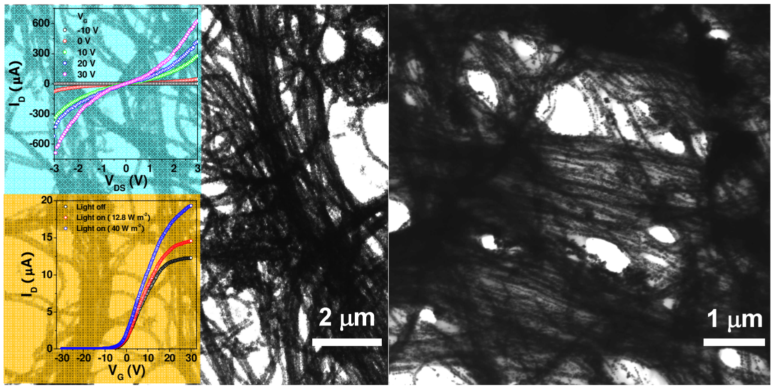

A series of one-dimensional assemblies of semiconductor nanocrystals with the enhanced field effect transistor performance have been studied.